Effect of Welding Speed in High Speed Laser-TIG Welding of Magnesium Alloy

Chenbin Li, Minghua Chen, Shengtao Yuan, and Liming Liu

Key Laboratory of Liaoning Advanced Welding and Joining Technology, School of Materials Science and Engineering, Dalian University of Technology, Dalian, China

In order to investigate the effect of welding speed on microstructures and mechanical properties in high speed welding, low power laser-tungsten inert gas (laser-TIG) hybrid welding process is proposed on AZ61 magnesium alloy. Defect-free welds are produced by employing welding speed ranging from 2,000 mm/min to 6,000 mm/min. It is found that welding speed has a significant influence on microstructures and mechanical properties of the joints. Results indicate that with rapid increasing of welding speed, both the liner energy and average grain size decrease on the premise that fully-penetrated joints with no macroscopic porosities or cracks are obtained. The microhardness in the weld fusion zone increases with the welding speed. It is also found that the tensile strength decreases after an increase with the increase in welding speed. The fracture mode changes from mixture fracture of ductile and brittle to typical intergranular fracture feature.

Keywords Hardness; Liner-energy; Microstructures; Speed; Tensile-strength; Welding.

Introduction

Welding is an important link in industrial production, and enhancement of welding efficiency has its own important function in increasing productivity. With the rapid development of manufacturing, traditional welding process can hardly meet industrial special demands towards high efficiency welding. As the inevitable demand and development trend of modern welding technology, raising the welding efficiency can be achieved by increasing welding speed or deposition efficiency [1].

Increasing welding speed is the key to improve welding productivity for thin sheet [2]. However, the increase in welding speed may bring about a variety of welding defects, ranging from undercut to lack of fusion to humping bead, which restrains the actual application of the joints [3]. In the context of welding mechanization and automation, increase of welding speed is the key step to develop potential productive forces to the full.

As the lightest structural material available so far, magnesium and its alloy are widely used in aircraft, automotive, and other fields due to their low density, excellent specific strength and sound damping capabilities, hot formability, and recyclability [4–7]. Arc welding and low power laser beam welding have been used for joining magnesium alloys, but the welding speed is slow [8–10]. The laser-tungsten inert gas (laser-TIG) hybrid welding is a new technology for magnesium alloys to realize high speed welding. There have been a number of valuable studies on laser-TIG hybrid welding of magnesium alloys. However, most of the welding speeds are less than 2,000 mm/min [11, 12]. In this article, the weldability tests have been performed on thin sheets of magnesium alloy AZ61 using low power laser-TIG hybrid welding at the welding speed ranging from 2,000 to 6,000 mm/min. Meanwhile, the effect of welding speed on microstructures and mechanical properties of the joints is investigated. The study is not only of important theoretical value, but also has practical implications for raising welding efficiency.

Experiment setup

Magnesium alloy AZ61 sheets with the dimension of $300 \times 100 \times 2\,mm^3$ were butt welded. The chemical composition of this alloy is 5.8–7.2 wt% Al, 0.4–1.5 wt% Zn, 0.2–0.5 wt% Mn, and balance Mg. Multimode Yttrium Aluminum Garnet (YAG) laser was used in the present experiment, and the pulse laser with the wavelength of 1.064 μm was focused through a lens with the focal length of 120 mm. The defocusing distance of laser beam to the surface of workpiece was 0 mm, and the spot diameter on the surface of workpiece was about 0.4 mm. The diameter of the tungsten electrode was 3.2 mm, and the angle between the electrode and the laser beam was 45°. The grease and residue on the surface of base metal (BM) were removed with acetone, and the oxidation film was also removed with emery cloth and stainless steel brush before welding. The current and voltage of TIG arc and laser power under optimized parameters are detected and acquired in real-time.

After welding, the specimens were cross-sectioned, ground, and polished. The microstructures were characterized by scanning electron microscope (SEM). The

joints were machined into tensile specimens, and tensile tests were carried out on CSS-2205 tensile machine at a cross-head velocity of 5 mm/min. The fracture surfaces were also observed with SEM. The hardness of the butt joints was measured using a Vickers microhardness tester with a 100-gram load for a 15-second dwell time.

RESULTS AND DISCUSSION

Weld Seam Morphology

Figure 1 shows the cross-sections and surfaces of weld joints produced with the optimized parameters, which are assessed based on the criterion below: the joint is fully penetrated, while no microscopic crack or pore forms at different welding speeds. It can be seen from the middle column of Fig. 1 that all the weld joints are fully penetrated. The surfaces of welds show clearly that the surfaces are smooth, clean, and continuous without the defects of surface porosity and crack. Because of the small BM thickness and high welding speed, underfill and over penetration are inevitable in the one side welding process without top filler wire or back forcible figuration. All the following discussions are on the basis of full-penetration and good formation of weld joints.

Welding Liner Energy

The current and voltage of TIG arc are detected and acquired in real-time, using ANALYSATOR HANN-OVER AH in welding process. Meanwhile, the laser power is measured, and the welding liner energy E can be calculated by

$$E = \frac{P_{Laser} + p_{Arc}}{V} = \frac{P_{Laser} + U \cdot I}{V}, \tag{1}$$

where P_{Laser} is the laser power, p_{Arc} is the TIG arc power, V is the welding speed, U is the average voltage of TIG arc, and I is the average current of TIG arc. Though fully-penetrated joints with good formation are obtained, there are great differences in welding liner energy, which directly influence the microstructures and mechanical properties.
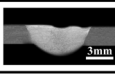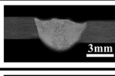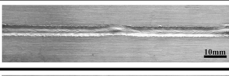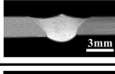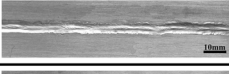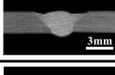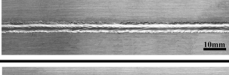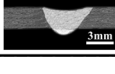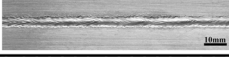

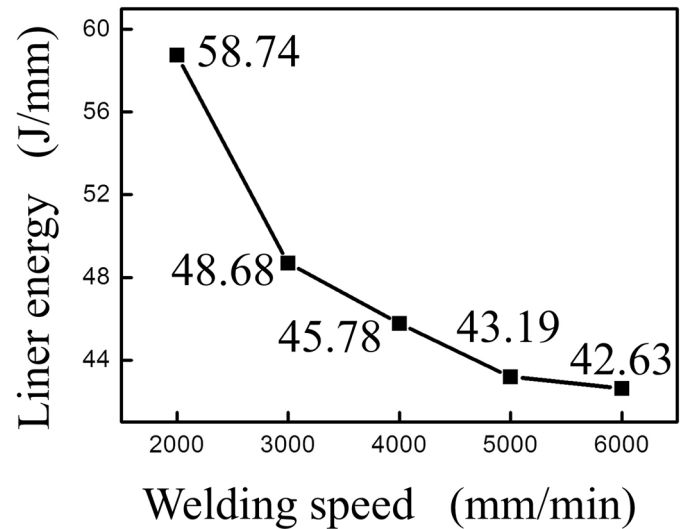| Welding speed (mm/min)	Cross-sections of weld joints	Surfaces of weld joints	Laser power (W)	Arc current (A)
2000			252	130
3000			393	160
4000			503	190
5000			629	210
6000			755	230

FIGURE 1.—Cross-sections and surface of welds.

FIGURE 2.—Relationship between liner energy and welding speed.

Figure 2 shows the relationship between liner energy and welding speed. It can be seen that the liner energy is 58.74 J/mm when the welding speed is 2,000 mm/min. min. As the welding speed reaches 6,000 mm/min, the liner energy drops to 42.63 J/mm. As shown in Fig. 2, it is obvious that the liner energy decreases with the increase of welding speed. Though fully-penetrated joints are obtained, the liner energy is significantly different. The reasons are given as follows: first, the arc current increases with the welding speed, and the arc force rises accordingly, which contributes to the heat conduction in depth; secondly, the increase of welding speed benefits the melting efficiency for the arc, and hence the energy utilization ratio increases [13]; thirdly, the higher the welding speed is, the higher the temperature is, and the absorptivity to the laser increases with the increase of the temperature of the molten pool surface [14].

Microstructures

Figure 3 shows the typical microstructures of the middle area of fusion zone (FZ) of weld joints at various welding speeds. The as-welded fusion zones all exhibit equiaxed crystal, but there is a big difference in grain size. Besides, precipitates always appear at the grain boundary, and they are dispersive, uniform, and mostly granular. According to related literature [15–17] and Mg-Al binary phase diagram, the precipitates presented in the weld bead always are β-$Mg_{17}Al_{12}$. As shown in Fig. 3, the faster the welding speed is, the finer the precipitates are; thus, they are beneficial to inhibit grain growth efficiently. The precipitates are of great advantage to improve the properties of the weld beads. As shown in Fig. 2, the welding liner energy decreases with the increase in welding speed, and the cooling rate ω_C can be expressed as

$$\omega_C = -2\pi\lambda c\rho \frac{(T_C - T_0)^3}{(E/\delta)^2}, \tag{2}$$
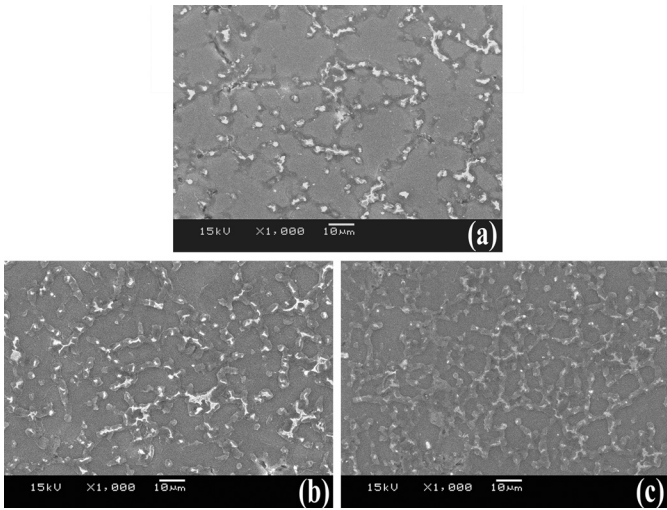
FIGURE 3.—SEM microstructures of FZ of weld joints at various welding speeds: (a) 2,000 mm/min; (b) 4,000 mm/min, and (c) 6,000 mm/min.

where λ is thermal conductivity, c is specific heat capacity, ρ is material density, T_c is the instantaneous temperature of weld metal, T_0 is the initial temperature of BM, δ is the thickness of base metal, and E is the welding liner energy. It can be deduced from Eq. (2) that cooling rate ω_C increases with the decrease in liner energy E. Based on the solidification theory, the higher cooling rate leads to the finer structures. When welding speed is 2,000 mm/min, the grain size of the FZ is about 30–40 μm (Fig. 3(a)). With the increase in welding speed, the grain size reduces to 8–10 μm at the welding speed of 6,000 mm/min (Fig. 3(c)).

As shown in Fig. 4, cracks are found in weld seam when the welding speed increases up to 5,000 mm/min and 6,000 mm/min. As is known, high strain rate is the main reason generating the crack [18]. According to Eq. (3) deduced from Eq. (2),

$$\frac{\partial e(t)}{\partial t} = \alpha \frac{2\pi\lambda c\rho(T_c - T_0)^3}{E/\delta}, \tag{3}$$

where term $\frac{\partial e(t)}{\partial t}$ is the strain rate of weld metal and α is linear expansion coefficient, it can be deduced that the smaller the welding liner energy is, the higher the strain
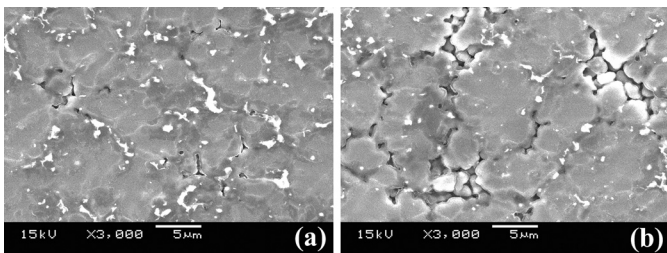

FIGURE 4.—Cracks in weld seam at different welding speeds. (a) 5,000 mm/min and (b) 6,000 mm/min.

rate is. When the welding speed is high, the welding liner energy is low and the tendency to form crack is high. In the course of solidification, the unset liquid metal is cut apart into several independent molten pools when the rising crystal interlace with each other. High cooling rate will result in easier formation of interdendritic shrinkage and interdendritic porosity, which may affect the mechanical properties.

Hardness

Particular attention is given to weld metal mechanical properties by monitoring the hardness. The results of microhardness measurements in the middle of FZ are shown in Fig. 5. Each of the results is the mean value of five specimens, and the fluctuation is little. The results show that microhardness increases with welding speed. When the welding speed is relatively low (2,000 mm/min), the average microhardness is 73.82 Hv. When the welding speed is up to 6,000 mm/min, it reaches 86.28 Hv. This can be explained by the Hall–Petch equation:

$$H_V = H_o + k \cdot d^{-\frac{1}{2}}, \tag{4}$$

where H_V is the microhardness of materials, H_o and k are constants, and d is the average grain size. The equation indicates that the grain refinement leads to the increase of microhardness.

Tensile Properties

Considering the influence of weld bead shape on the tensile properties, samples were polished into 1.5 mm in thickness, and standard tensile specimens as shown in Fig. 6(a) were manufactured based on ISO 4136:2001 Standards before tensile test. A total of five specimens under every designated welding speed were tested. All the specimens fractured in the weld beads and the tensile specimens after testing were also presented in Fig. 6(b).
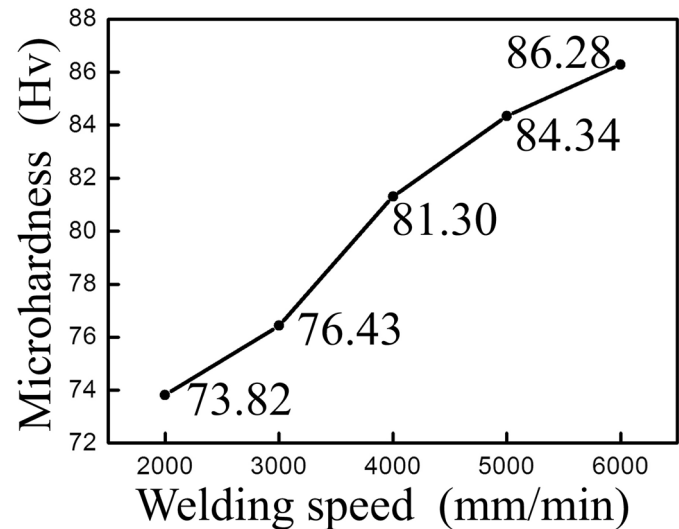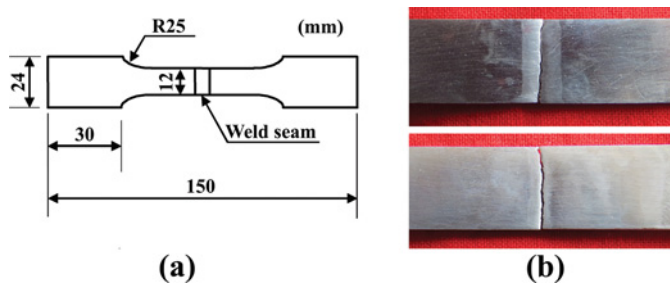

FIGURE 5.—Microhardness in FZ.

FIGURE 6.—Geometry of standard tensile specimen (a) and tensile specimen (v = 6,000 mm/min) after testing (b) (color figure available online).

Figure 7 is the graph on the relationship between the welding speed and tensile strength, and each of the tensile strength results is the mean value of five specimens. The standard deviations are calculated, and they are 18.32, 16.18, 8.39, 10.94, and 9.55, respectively, as the welding speed increases from 2,000 mm/min to 6,000 mm/min. Based on another form of the Hall–Petch equation,

$$\sigma_s = \sigma_o + k \cdot d^{-\frac{1}{2}}, \qquad (5)$$

where σ_s is the strength of materials, σ_o and k are constants, and d is the average grain size, the strengthen should increase as the welding speed increases. However, the results do not follow up the above rule. The results show that the tensile strength of BM is considerably higher than that of weld joints. The tensile strength decreases after an increase with the increase of welding speed and tends to the peak at 270.30 MPa, which is about 95% of that of BM (285.33 MPa), at the welding speed of 4,000 mm/min. The reason for the first increase of tensile strength is grain refinement, while that for the decrease may be welding defects forming in welding process.

Figure 8 shows the fracture surfaces of the specimens using SEM. As it can be seen in Fig. 8, the fracture surface of the BM mainly exhibits the features of a
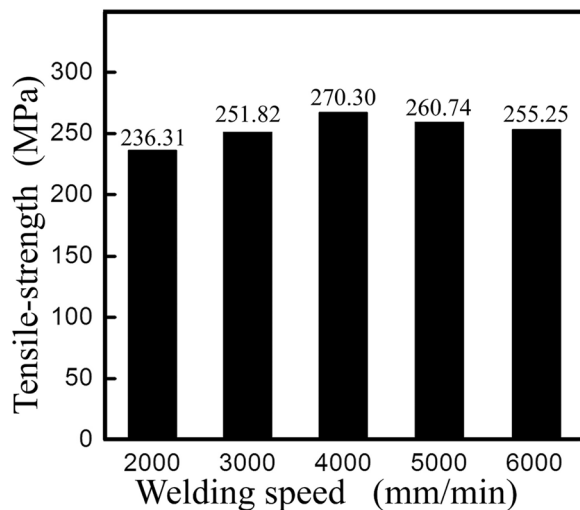

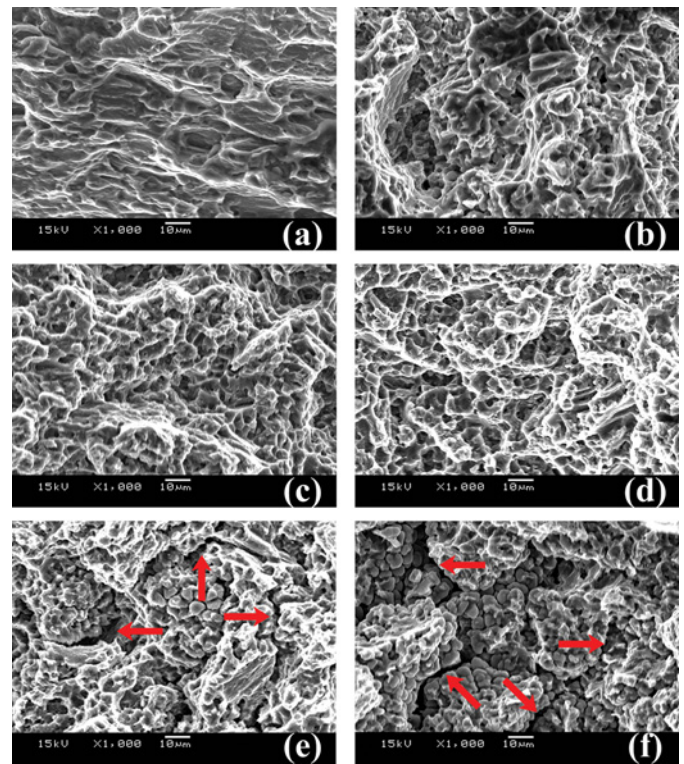FIGURE 7.—Tensile strengthen of welded joints.

FIGURE 8.—Observations on fractured surfaces of BM and welds at different welding speeds: (a) BM; (b) 2,000 mm/min; (c) 3,000 mm/min; (d) 4,000 mm/min; (e): 5,000 mm/min; and (f):, 6000 mm/min (color figure available online).

ductile fracture, which is characterized by more tearing fibers and ridges (see Fig. 8(a)). Seen from Figs. 8(b)–(d), the tensile fractures are mixture of ductile and brittle. However, the size of dimple becomes larger and bigger in Figs. 8(b)–(d), and meanwhile the direction of dimple is becoming inclined, indicating that the plasticity increases gradually. This is because the grain size decreases with the increase in welding speed. Seen from Figs. 8(e),(f), the fracture surface morphologies display a typical intergranular fracture features and they are taken as typical brittle fracture features. Besides, microcracks (marked with arrows in Figs. 8(e),(f)), which can reduce the strength, exists on the fracture surface of the weld joints.

CONCLUSION

High-speed laser-TIG hybrid welding is conduced and defect-free welds are produced at the welding speeds ranging from 2,000 mm/min to 6,000 mm/min. The experimental results lead to the following conclusions.

1. Under the precondition that fine and full-penetrated weld seams are obtained, the welding liner energy decreases with the increase in welding speed.
2. With the increase in welding speed, the average grain size in the FZ of weld seam decreases and the microhardness in the FZ increases.
3. The tensile strength decreases after an increase with the welding speed, and the joint strength reaches a

maximum value of 270.30 MPa (about 95% of that of BM). The fracture mode changes from mixture fracture of ductile and brittle to typical intergranular fracture feature.

REFERENCES

1. Celanovic, N.; Boroyevich, D. A comprehensive study of neutral-point voltage balancing problem in three-level neutral-point-clamped voltage source PWM inverters. *IEEE Trans. on Power Electronics* **2001**, *15* (2), 242–249.

2. Kammerhuber, C.; Sommerfeld, R. High deposition MAG welding: Used for welding bridges and structures. *Welding in the World* **1996**, *38* (1), 337–343.

3. Mendez, P.F.; Eagar, T.W. Penetration and defect formation in high-current arc welding. *Welding Journal* **2003**, *82* (10), 296–306.

4. Qiu, R.; Shi, H.; Yu, H. Effects of electrode force on the characteristic of magnesium alloy joint welded by resistance spot welding with cover plates. *Materials and Manufacturing Processes* **2010**, *25* (11), 1304–1308.

5. Chen, Z.-H.; Cheng, Y.-Q.; Xia, W.-J. Effect of equal-channel angular rolling pass on microstructure and properties of magnesium alloy sheets. *Materials and Manufacturing Processes* **2007**, *22* (1), 51–56.

6. Chen, Q.; Yan, H.; Chen, J.; Zeng, P.; Yu, Z.; Su, B. Laser beam welding of AZ31 magnesium alloy with filler strip. *Materials and Manufacturing Processes* **2010**, *25* (11), 1227–1232.

7. Zhang, Z.; Zhang, F. Spectral analysis of welding plasma of magnesium alloy using flux coated wire. *Materials Transactions* **2009**, *50* (8), 1909–1914.

8. Manti, R.; Dwivedi, D.K. Microstructure of Al-Mg-Si weld joints produced by pulse TIG welding. *Materials and Manufacturing Processes* **2007**, *22* (1), 57–61.

9. Zhu, T.; Chen, Z.W.; Gao, W. Microstructure formation in partially melted zone during gas tungsten arc welding of AZ91 Mg cast alloy. *Materials Characterization* **2008**, *59* (11), 1550–1558.

10. Quan, Y.J.; Chen, Z.H.; Gong, X.S.; Yu, Z.H. Effects of heat input on microstructure and tensile properties of laser welded magnesium alloy AZ31. *Materials Characterization* **2008**, *59* (10), 1491–1497.

11. Liu, L.; Hao, X. Lower power laser-TIG hybrid welding process of magnesium alloy with filler wire. *Materials and Manufacturing Processes* **2010**, *25* (11), 1213–1218.

12. Song, G.; Luo, Z. The influence of laser pulse waveform on laser-TIG hybrid welding of AZ31B magnesium alloy. *Optics and Lasers in Engineering* **2011**, *49* (1), 82–88.

13. Kou, S. *Welding Metallurgy*; Wiley: Hoboken, NJ. 2003.

14. Sun, H.; Song, G.; Zhang, L.F. Effect of oxide activating flux on laser welding of magnesium alloy. *Science and Technology of Welding and Joining* **2008**, *13* (4), 305–311.

15. Song, G.; Wang, P. Pulsed MIG welding of AZ31B magnesium alloy. *Materials Science and Technology* **2011**, *27* (2), 518–524.

16. Huang, C.J.; Cheng, C.M.; Chou, C.P. The influence of aluminum content of AZ61 and AZ80 magnesium alloys on hot cracking. *Materials and Manufacturing Processes* **2011**, *26* (9), 1179–1187.

17. Marya, M.; Edwards, G.R. Influence of laser beam variables on AZ91D weld fusion zone microstructure. *Science and Technology of Welding and Joining* **2002**, *7* (5), 286–293.

18. Parsons, M.; Stepanov, E.V.; Hiltner, A.; Baer, E. Effect of strain rate on stepwise fatigue and creep slow crack growth in high density polyethylene. *Journal of Materials Science* **2000**, *35*, 1857–1866.